

Surface and sub-surface modifications of copper electrodes exposed to high-field conditioning at cryogenic temperatures.

Marek Jacewicz^a, Iaroslava Profatilova^a, Piotr Szaniawski^a, Inna Popov^b, Yinon Ashkenazy^b, Sergio Calatroni^c, Walter Wuensch^c

^a*Department of Physics and Astronomy, Uppsala University, Uppsala, Sweden*

^b*Recah Institute of Physics, The Hebrew University of Jerusalem, 9190401 Jerusalem, Israel*

^c*CERN, European Organization for Nuclear Research, 1211 Geneva, Switzerland*

Abstract

In order to investigate the dependence of conditioning and field-holding on temperature, three pairs of copper electrodes underwent high voltage conditioning with direct current (DC) pulses while kept at a single temperature, unique for each set (300 K, 30 K and 10 K), until saturation field for each set was found. The sets conditioned at cold showed a significant increase in the field holding capability, reaching fields up to 147 MV/m after tens of millions of pulses and very few breakdowns (BDs). We interpret this as an indication of the conditioning effect being due to high field pulsing rather than exposure to BDs. The effect of the warm and cold conditioning was investigated with high-resolution microscopy, characterizing the BD spots on the anode and cathode according to their morphology and with scanning transmission electron microscopy (STEM) analyzing the changes in the sub-surface regions. Atypical BD spot features were found on the cryogenically conditioned cathode surfaces, with very shallow craters of a star-like shape. The number of atypical spots increased with decreased temperatures, reaching 26 and 53 percent of the total number of spots at 30 K and 10 K, respectively. A hypothesis explaining the formation of these features is also presented. The very different morphology of the anode and cathode BD spots is presented in details that suggest an unknown shielding mechanism that prevents the center of the anode spot from melting. These results provide important experimental input for the development of quantitative theories and models for BD initiation and inter-electrode plasma formation.

1. Introduction

High electrical fields in ultra-high vacuum environments (UHV) are needed in many areas of research and for many technologies, such as high energy accelerators, high vacuum interrupters, fusion research, electron and X-ray sources and space applications [1, 2]. The upper limit to which electrodes can hold an electric field is a main consideration in the design and operation of various systems. It has been observed that when high electrical field pulses are applied to the surface repeatedly, the accepted electrical field increases [3, 4]. A traditional explanation for this conditioning process is that the sharp features on the electrode surface are destroyed during the breakdown (BD), and so higher fields can be applied to the surface without further breakdowns. But experimental data shows that this is not a complete explanation. Firstly, even very smooth surfaces, if unconditioned, will eventually experience breakdowns at a given field, but will accept higher fields after conditioning, with the much rougher surface covered by the breakdown craters. Moreover, the maximum field that a metal surface can tolerate correlates well with its crystal structure [3, 5]. Furthermore, in [4], it has been shown that the conditioning effect correlates to the number of applied pulses, and not with the number of breakdowns, suggesting that the conditioning is an effect

of pulses, and not of breakdowns. Breakdowns are, at best, a way of measuring the conditioning state of a surface.

A more complex picture has emerged, in which there are extrinsic and intrinsic mechanisms responsible for the breakdown generation [6–9]. The former are aforementioned irregularities or contamination of the electrode surface. The latter mechanism is related to the material properties and alters the breakdown rate even when the effect of extrinsic processes was exhausted by cleaning of the surface via initial "processing" by plasma from discharges. The research into the mechanisms behind intrinsic breakdown generation has been an active field of study for many years, and gained renewed interest over the last decade. In recent years, theoretical models concentrated on trying to link pre-breakdown plastic activity at a metallic surface exposed to high field to the formation of a localized specific feature, which will nucleate the ensuing breakdown. Various options for such local evolution were studied, including local dislocation activity [10, 11]. These stress driven processes have a characteristic thermal activation energies which lead to an exponential temperature dependence of breakdown rates, this respectively of the exact nature of the specific defect reaction [12, 13].

Recently an effective kinetic mean-field model, describing the evolution of a self-interacting dislocation pop-

ulation, led to a similar dependence even when self-interactions between dislocations and various obstacles is taken into account [14]. Indications to the validity of this description were found in measurements of pre-breakdown dark current fluctuations, which are consistent with the dynamics depicted in the model. The measured distribution fits well with the model prediction [15, 16]. However, due to experimental difficulties, as of now there is no direct observation linking specific dislocation activity to breakdowns, and we are left with non-direct measurements [17].

Since most kinetic models include a thermally activated process, observing temperature dependence of breakdown processes is expected to offer a significant change in breakdown properties, which can be measured and used to constrain various theoretical models [15].

Studies have shown that using cold temperatures will affect the conditioning by largely increasing the maximal attainable fields on the surface. These changes are predicted by the kinetic models described above. However, it is noteworthy that changes in material properties such as hardness, thermal conduction, and thermal expansion coefficients may lead to such changes even if these models do not hold. The role of the cryogenic temperatures on the BD rate have been verified experimentally both in radio-frequency (RF) and in DC studies [18, 19].

In this paper, we present a study combining the investigation of the intrinsic and extrinsic mechanisms by observing surface modification due to conditioning in cryogenic temperatures under very high fields. Since the conditioning has been linked to a process of microstructural hardening caused by the stress associated with the applied electric field [9], we compare samples conditioned exclusively at warm or cold temperatures using various microscopy techniques to characterize the sub-surface and the surface features found on the samples.

2. Methodology

2.1. Electrodes

Results reported here are from measurements on three OFE copper samples (Table 1). Electrodes were produced from copper UNS C10100 Grade 1, which was proposed in the past as a candidate material for high gradient RF cavities [20]. The electrodes were produced using fly-cut followed by diamond turning, achieving surface roughness of less than 25 nm. All electrodes were cleaned with chemical solvents, according to a previously established protocol [21]. The samples were not high-temperature-treated and one can still observe grooves after diamond machining on the surface as well as individual copper grains with sizes of 20-80 μm .

All the electrode pairs have the same geometry, with the high field area defined by the size of the anode of 40 mm diameter. During the experiments, the electrodes are separated by a ceramic spacer (Al_2O_3) with high dielectric strength. The spacer and the electrodes are ma-

chined very precisely, guaranteeing very high level of parallelism.

2.2. Conditioning

The electrode set 007-Cu was conditioned at CERN's DC discharge system [22, 23], while the sets 038-Cu and 052-Cu at Uppsala's cryogenic discharge system [19]. The systems share the design of the high voltage (HV) scheme and the conditioning procedure that was developed for the RF and DC tests for CLIC project [22–24]. The cryogenic system in Uppsala, however, can cool the samples down to 4 K for the tests.

During the conditioning, HV pulses with 1 μs width and 1 kHz repetition rate were used for the conditioning at cold and 2 kHz for 007-Cu¹. The change in the repetition rate is not expected to have any significant impact on the experiment [25]. The conditioning tests were done using breakdown-rate feedback mode, meaning that the HV was ramped up or down over time while monitoring the breakdown rate in order to keep it at 1×10^{-5} BD/pulse, see [23] for details². Each electrode set was conditioned only at a single temperature, the 007-Cu at room temperature, while the 038-Cu and 052-Cu were directly cooled down to 30 K and 10 K respectively for the test.

2.3. Analysis

In order to better understand the effect of the conditioning with high electric field, at distinct temperatures, different analysis methods were used to search and analyze the modification in the sub-surface regions and on the surface of the electrodes. The methods include high resolution light microscopy as well as Scanning Transmission Electron Microscopy (STEM). Even though the breakdown reaction is presumably initiated from the cathode, during the discharge phase, a plasma channel is formed between the electrodes, and both anode and cathode surfaces are affected. Therefore, analyses of both electrodes are of interest.

2.3.1. Large scale structures and breakdown spot matching

Global microscopic observations of breakdown features on anode and cathode were done using SmartScope FLASH 200 light microscope at Uppsala University. First, the corresponding areas on anode and cathode were scanned with 1 $\mu\text{m}/\text{px}$ resolution. The single scans were then stitched together to form a larger map. Next, the analysis of the larger maps was done using a dedicated MATLAB script, similar to one described in [22]. An automatic circle-finding routine was used at the initial stage to create an array with the coordinates of the recognized surface features with first estimate for the circles' radii. A link between the anode and cathode images and coordinates was done semi-manually and resulted in a set of

¹The lower repetition rate at cold was used to maintain the stable temperature.

²Breakdown rate is calculated using an exponentially weighted moving average method over a 1 million pulses window.

the transformation factors (a scale, a rotation angle and translation x and y positions) that allowed for direct comparison of the features on anode and cathode for the same breakdown, see fig. 1.

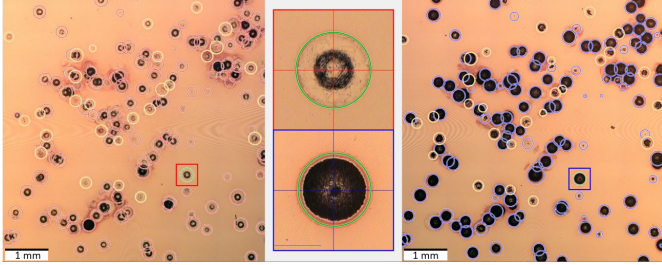


Figure 1: The figure presents semi-automatic breakdown counting software with anode-cathode breakdown-site matching. The anode is on the left, the cathode is on the right. In the middle, a zoom of the selected site on the anode (top) and cathode (bottom) is shown. Presented data come from 038-Cu set.

2.3.2. Sub-surface analysis

The conditioned hard copper samples were analyzed with a high angular annular dark field (HAADF) STEM imaging to identify variations induced in their sub-surface structure at field exposure. This was done with Scanning-Transmission Electron Microscope (S)TEM Tecnai F20 G2 operated at 200 kV and equipped with Fischione HAADF STEM detector. For comparison, cross-sectional lamellas were extracted with a Focused Ion Beam (Dual Beam FIB Helios Nanolab 460F1) from the reference regions and the regions that were exposed to the highest electrical field. The reference region is the region that underwent the same initial treatment, but was not exposed to high fields (see fig. 2 for the illustration). The analysis of the STEM data included counting dislocations and calculating a local dislocation density.



Figure 2: A schematic view of the electrodes under test. On the left: view from the side. On the right: top view, with a definition of different regions (valid for anode and cathode): reference - the region with no field (orange), high field region (red) and breakdown site (small black circle).

3. Results

3.1. High-voltage BD behavior during conditioning

Typically, during the conditioning, the samples should reach stable field level with a BD rate below 1×10^{-5} BD/pulse. This value, calculated by averaging over the

last 10 million pulses, is called the saturation field. Due to the stochastic nature of the conditioning process, before the saturation field is reached, the fields can fluctuate at different levels. These fluctuations are of interest, and one of the factors that can describe it is the overall maximum attained field and number of pulses and BDs needed to reach that field. The comparison of the conditioning curves for all the samples is shown in fig. 3 and the main information extracted from the measurements is given in table 1. The automatic conditioning algorithm dictates the constant slope visible during the first part of the conditioning, as voltage is ramped at a constant rate.

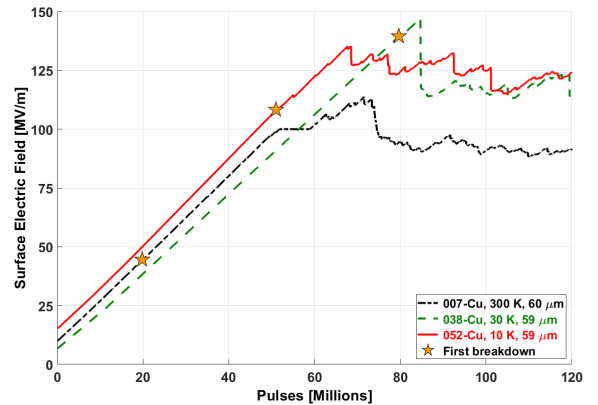


Figure 3: Comparison of conditioning curves for sample: 007-Cu at 300 K (black dashed-dotted line), 038-Cu at 30 K (green dashed line) and 052-Cu at 10 K (red solid line). A yellow star on the conditioning curve indicates the pulse number corresponding to the occurrence of the first breakdown.

3.2. Characteristics of common surface features of the breakdown sites

BD events lead to the formation of crater-like features on metallic surfaces on both sides of the event [26]. Cathode and anode surfaces were analyzed using microscopy to characterize these typical features, and damaged areas were categorized. Specific events were identified using the procedure described in section 2.3.1.

Fig. 4a shows a typical "crater" left after a breakdown on an anode, with a halo around the center due to a capillary wave formed in a molten state. It is maximum $0.5 \mu\text{m}$ deep, with tiny machining grooves still visible over all radius [27]. A typical round-shape anode BD feature is composed of a *reflective central part*, r_a (a green solid line), surrounded by a *rough circular region*, w_a (a red dashed line), with a *lighter circular region*, tlr_a (a purple square dotted line), around.

Meanwhile, a typical cathode BD feature has a *large dark rough circular region*, w_c (a red dashed circle), and a *thin lighter ring*, tlr_c (a purple dotted circle), shown on fig. 4b. The cathode BD feature has usually $1 \mu\text{m}$ depth in the center (from reference [27]) and looks darker over all crater area (fig. 4), than on the anode. The machining grooves are not visible on BD cathode site, probably

Table 1: Main parameters for the tests.

Electrodes	Temperature [K]	Gap [μm]	First BD E_{field} [MV/m]	Max E_{field} [MV/m]	Saturation E_{field} [MV/m]	Nb of BDs to max E_{field}
007-Cu	300	60 \pm 3	46 \pm 3	114 \pm 6	90 \pm 5	94
038-Cu	30	59 \pm 3	140 \pm 8	147 \pm 8	120 \pm 7	7
052-Cu	10	59 \pm 3	108 \pm 5	135 \pm 7	123 \pm 7	27

because of high temperature on site during BD and deep damage. We found emitted jets in random radial directions around BD crater, again typically only for the cathode side (fig. 4b).

3.3. Star-like BD features

On the samples tested at cold a number of atypical BD features were discovered. The spots are characterized by a very shallow depth with star-like shape instead of circular one. The star-like BDs occurred on the cathode only. See the SEM image on fig. 5 for details of the star-like BD morphology.

More examples of atypical BD features are shown on fig. 6. The spots are spatially matched, with the top and bottom row showing features from the same breakdown on anode respectively cathode. The same feature characterization as before was done for the atypical spots. Figs. 6a and 6d demonstrate how the regions for star-like BD features are defined, similarly to the regular BDs, described earlier (see figs. 4a and 4b).

The anode BD feature corresponding to the same cathode spot looks very regular. One finds a light central disk with a halo around it (fig. 6b). On average, the anode spots corresponding to star-like cathode sites are smaller and more shallow, with details faintly visible (fig. 6c). The machining grooves are also still visible under the feature.

3.4. Statistical analysis

The high resolution scans of the cathode and anode surface were analyzed with the software mentioned in section 2.3.1 matching the corresponding BD spot with close to 100% accuracy. Afterward, the regular and atypical features were characterized looking for similarities and differences, and quantifying the relationship between the temperature and number of different classes of BDs.

3.4.1. Regular features

The ratios between different anode and cathode features were studied in details mostly for the electrode set 038-Cu and 052-Cu and summarized in table 2. For 007-Cu, only average radii sizes are presented, as the craters on cathode and anode were not linked during analysis to each other and star-like features were not found at the room-temperature test.

The ratios between cathode and anode radii found for the cold sets are very similar, agreeing within the uncertainties. For example, the ratio for the rough dark circular regions, w_c/w_a , to be 1.6 ± 0.3 for 038-Cu and 1.5 ± 0.2 for

052-Cu (also see fig. 7a) and the ratio between thin light rings radii of cathode and anode, tlr_c/tlr_a , was found to be around 1 (shown on fig. 7b).

3.4.2. Atypical features

The star-like features were only found on the cathodes of the samples that were tested at cryogenic temperatures. These BDs were counted and linked to each other on both electrodes, as before for regular sites.

After the initial analysis, a circle was fitted to each star-like spot to estimate the size. The comparison of the radii for anode and cathode spots is presented in table 3. Figure 7 includes results from all the features found on the 038-Cu surface where anode-cathode spots could be matched, including star-like spots. It shows that the distribution of radii of the BD features on the anode and the cathode changes depending on the region taken into account. For the rough circular regions, the difference is most noticeable, 70 - 150 μm for cathode vs 50 - 100 μm for anode. Meanwhile, for the same BD features, the radii for the regions of thin lighter rings, are nearly equal with distribution between 100 - 200 μm (fig. 7b). Fig. 7c compares the radii of rough circular regions for typical and star-like BD features, where again the distributions are very similar. Only cathode radii are compared, as it is difficult to determine the radii for weak spots on anode side (as shown on fig. 6c).

3.5. Sub-surface features

The conditioned copper samples were analyzed after field exposure to identify variations in their sub-surface structure. This was done by creating a HAADF STEM picture of cross-sectional lamellas which were created using field ion beam lithography. Lamellas taken from field exposed regions were compared to lamellas from reference regions, see fig. 2.

The reference sub-surface regions of cathodes 007-Cu and 038-Cu contained a rather high density of structural defects, which was induced by the diamond turning (fig. 8). Although grain structures seem to differ between samples, this can be attributed to the low-temperature treatment sample 038-Cu was exposed to, which generated a significant thermal load and is consistent with previous observations of grain refinement and strong surface effects on dislocation structure [28, 29]. In both samples, grain structure, and dislocations walls are observed to be continuous up to the surface. However, clear variation in structure can be observed in the conditioned regions. Conditioning

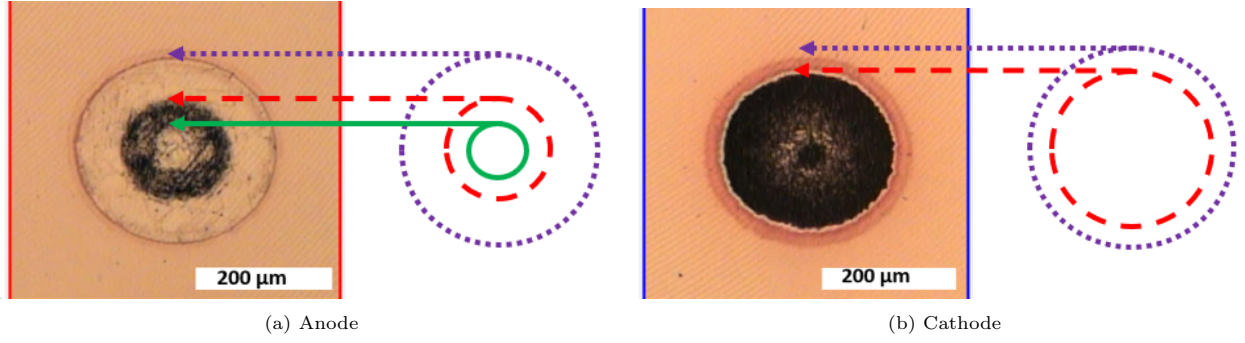


Figure 4: Typical BD features from a specific event: (a) Anode side: a round-shaped anode spot composed of a reflective central part (r_a , a green solid circle) surrounded by a rough circular region (with a radius of w_a , marked using a red dashed circle). The whole spot is surrounded in a lighter circular region with a radius of tlr_a and marked as a purple square dotted circle. (b) Cathode side: a cathodic spot composed of a large, dark, rough circular region (with a radius of w_c and marked using a red dashed circle) and a thin lighter ring (tlr_c , a purple dotted circle).

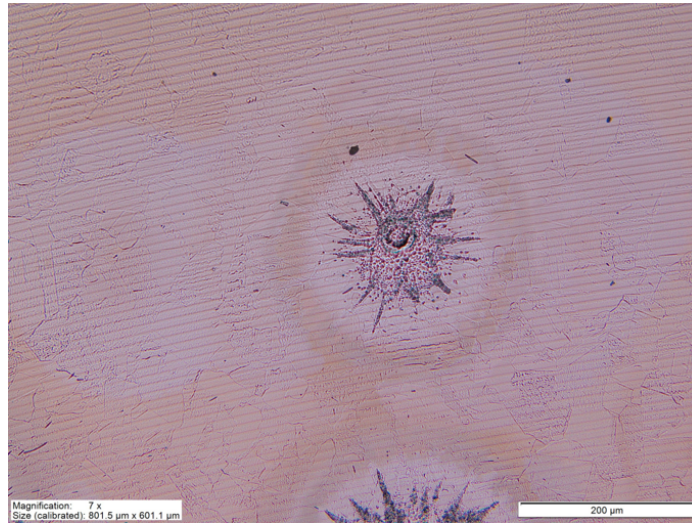


Figure 5: Details of the star-like BD morphology. Visible are also the machining grooves left after diamond turning processing.

Table 2: Average radii and ratios between sizes of BD features.

Type	Value	007-Cu	038-Cu	052-Cu
Regular	r_a	20 ± 4	21 ± 4	23 ± 3
	w_c/w_a		1.6 ± 0.3	1.5 ± 0.2
	tlr_c/tlr_a		1.0 ± 0.1	1.0 ± 0.1
	tlr_a/w_a		1.9 ± 0.3	2.0 ± 0.2
	tlr_c/w_c		1.2 ± 0.2	1.3 ± 0.2
	Average radius on cathode (w_c), μm	101 ± 20	125 ± 16	111 ± 16
Average radius on anode (w_a), μm	73 ± 12	78 ± 11	76 ± 10	
Star-like	w_c/w_a		1.6 ± 0.5	1.5 ± 0.1
	tlr_c/tlr_a		1.0 ± 0.1	1.0 ± 0.1
	tlr_a/w_a		1.7 ± 0.4	1.9 ± 0.2
	tlr_c/w_c		1.1 ± 0.2	1.3 ± 0.1
	Average radius on cathode (w_c), μm	–	109 ± 25	111 ± 14
	Average radius on anode (w_a), μm	–	70 ± 28	77 ± 8

Table 3: Main statistical information about the microscopic images.

Samples	Temperature	Nb of BDs	Nb of star-like pairs (and percentage)
038-Cu	30 K	145	37 (26 ± 5 %)
052-Cu	10 K	280	149 (53 ± 7 %)

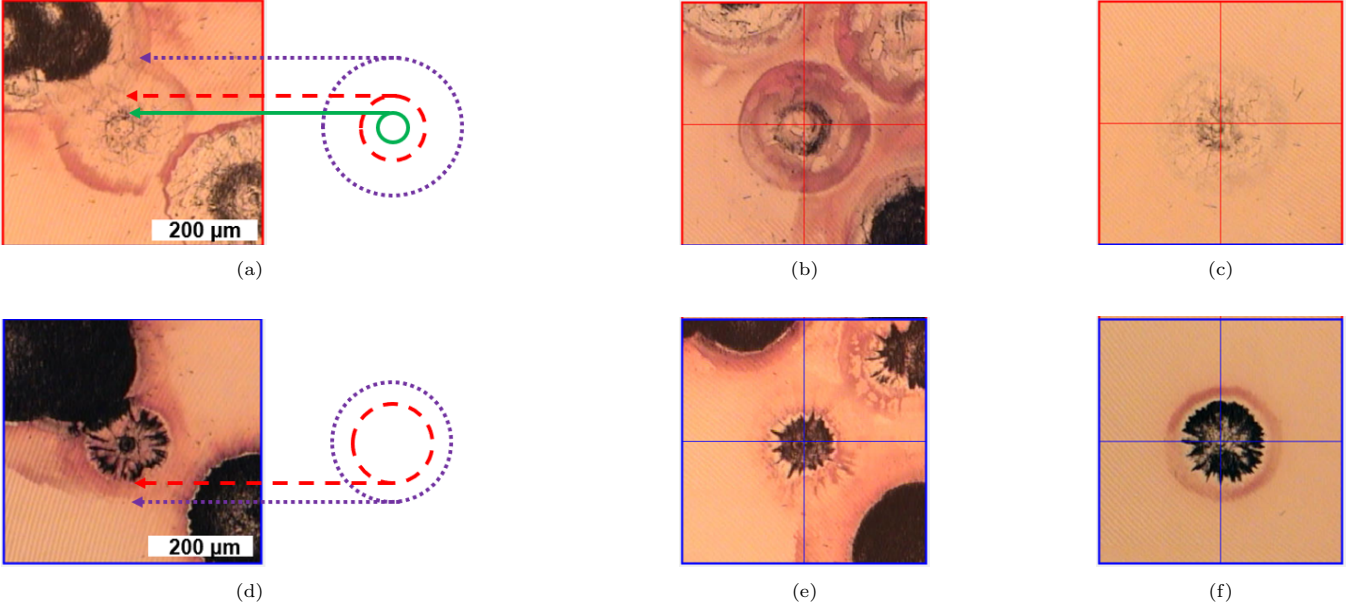


Figure 6: Breakdown features on the anode, top row, (6a-6c), and corresponded atypical feature found on the cathode (6d - 6f). On the left, 6a and 6d, definition of the regions used to characterize the star-like breakdown features. For the anode: a reflective central part (r_a , a green solid circle) surrounded by a rough circular region (w_a , a red dashed circle) with a lighter circular region (tlr_a , a purple square dotted circle) around. For the cathode: a large, dark, rough circular region (w_c , a red dashed circle) and a thin lighter ring (tlr_c , a purple dotted circle).

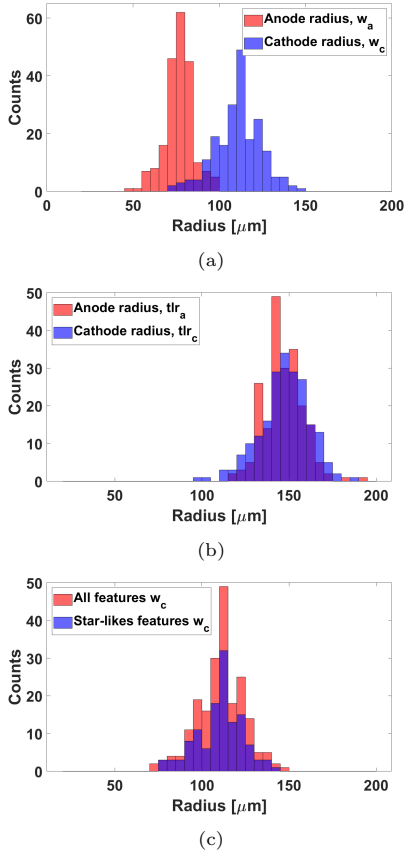


Figure 7: Comparison of radii for 052-Cu: (a) anode vs cathode for all BD features (dark rough circular region), (b) thin light rings for all BD features radii for anode and cathode, (c) star-like and the rest of BD feature on the cathode (dark rough area).

in both cases leads to a significant reduction in the number of dislocation walls (fig. 9). This effect is more pronounced in the cold-conditioned sample 038-Cu (fig. 10).

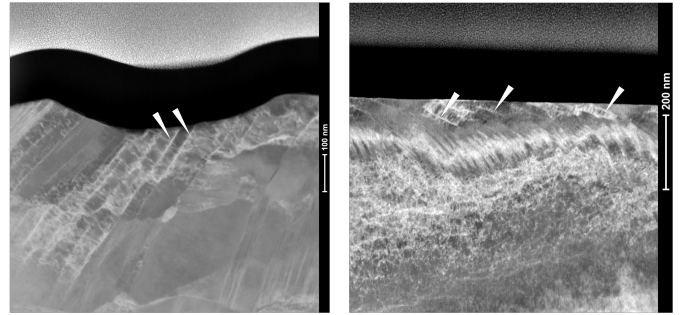


Figure 8: Cathode structure below the surface in reference regions. Images are from cathodes conditioned at room temperature (left, sample 007-Cu) and 30 K (right, sample 038-Cu). White arrows mark dislocation walls of sub-micron domains introduced by the diamond turning of cathode surfaces. Sample 007-Cu was cleaned by chemical etching, leading to a non-uniform removal of the top 100 nm.

3.6. Hardness

In addition to microscopy, Vickers hardness was measured for the copper sample conditioned at 30 K. Hardness was measured at two types of locations: area exposed to high field during conditioning but without visible breakdown site, and inside the breakdown spot - within the perimeter of molten copper. Measurements were done with a microhardness tester Duramin-40M3 (Struers) under 20 gf load and 10 seconds dwelling, and were repeated

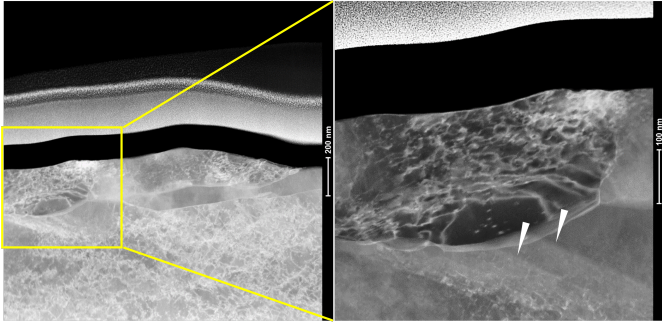


Figure 9: Subsurface structure in the field-exposed region of the sample 007-Cu conditioned at 300 K. The right panel is a magnified view of the region marked on the left one. White arrows mark the remaining dislocation walls.

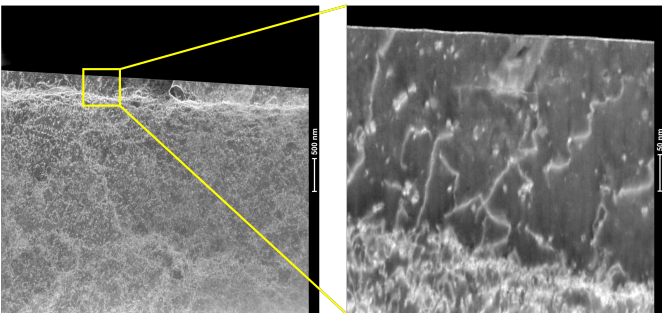


Figure 10: Subsurface structure in the field-exposed region of the sample 038-Cu conditioned at 30 K. The right panel is a magnified view of the region marked on the left one.

at 10 separate locations for each location type. Measurements were done separately at the center of the sample, up to a distance of 1 cm from the center of the electrode, within 1 cm from the outer region of the exposed area, and near the electrode edge which was not exposed to high field, see fig. 2. The results are presented in table 4. The hardness of the conditioned regions varied between 90 and 110 (HV) with lower values attained at BD sites and higher values in between these sites. These values are within the range of hardness attained at a reference outer region of the sample, which was not directly exposed to the same high fields. We note that the lower range of values was measured at sites where the surface was modified due to thermal effects, and cross-sectional microscopy showed formation of a recrystallized melted layer. All these values are considerably higher than 47 ± 3 (HV) [30], measured on a heat-treated sample of the same material, resulting in 'soft' copper with large grain size. See, for example, reference [9] for detail description of this treatment and results of conditioning. We therefore conclude that hardness as measured by this method is not directly linked to conditioning, or field retention ability of the surface.

4. Discussion

A series of measurements were carried out with three pairs of planar copper electrodes, all similarly manufac-

tured and treated. The sets underwent high-field conditioning with the identical effective gap size ($60 \mu\text{m}$) and following the same procedure until saturation field for the set was found. The conditioning involved repeated exposure to short high voltage DC pulses, allowing for occasional vacuum breakdown formation, resembling the operation of a high gradient RF cavity. The conditioning was performed at a single temperature, unique for each set, i.e. at 300, 30, and 10 K, respectively.

Conditioning at cryogenic temperatures led to a significant increase in the field holding capability of the electrodes, in agreement with previous observations [19, 31]. In addition to the difference in saturation values, the field where the initial BD event was observed increased significantly with the lowering of the working temperature of each electrode set. In the case of electrodes tested at room temperature, initial BD was observed after 20 million pulses at 45 MV/m , while the electrodes tested at 10 and 30K had the first BD occurring after 50 and 80 million pulses at 108 and 139 MV/m , respectively (see fig. 3). This observation is consistent with the previous hypothesis that high field pulsing rather than exposure to BDs serves to condition the sample [4]. To separate the effect of the conditioning from the hardening due to cryo-cooling we performed field emission scans after the cooling, but before the conditioning on 038-Cu. To avoid BDs, the emitted current was limited to tens of nano-amperes. When the pre-breakdown emission current between the electrodes is measured as a function of the applied voltage, a so-called Fowler-Nordheim plot is obtained, see figure 11a. By measuring the slope of the data plot, the local field enhancement factor β can be determined [32]. The macroscopic breakdown voltage V_M is related to the known critical local breakdown field E_{local} , believed to be an intrinsic parameter of the material and found to be 10.8 GV/m for copper [3]. Using

$$E_{local} = \beta \frac{V_M}{d} = \beta E_{macro} \quad (1)$$

where d is the gap size, and using the fitted value of $\beta = 96.3$, we obtain $E_{macro} = 112 \text{ MV/m}$, below the value where the first BDs occurred ($E_{macro} = 140 \text{ MV/m}$). We conclude that using just HV pulses, the surface was conditioned to a much higher field value than indicated by the field emission scan. In fact, soon after the BDs started to occur, the field holding diminished somewhat, staying at around 120 MV/m level. This effect of deconditioning has been observed before, but is not yet fully understood.

After the high-field conditioning at warm and cold, the microstructural changes in the electrode materials were investigated with a light microscope (surface) and STEM setup (subsurface). In the former case, the surface of the electrodes was photographed with high resolution, allowing to identification of imprints left by the BD event on the anode and cathode sides for all the BDs. Regular BD spots on anode and cathode were characterized according to their morphology. The measured sizes of each region

Table 4: Hardness of copper, Vickers number (HV).

Reference	Conditioned non-BD site		Conditioned BD site	
	center	edge	center	edge
104 ± 3	107 ± 4	108 ± 4	97 ± 6	93 ± 4

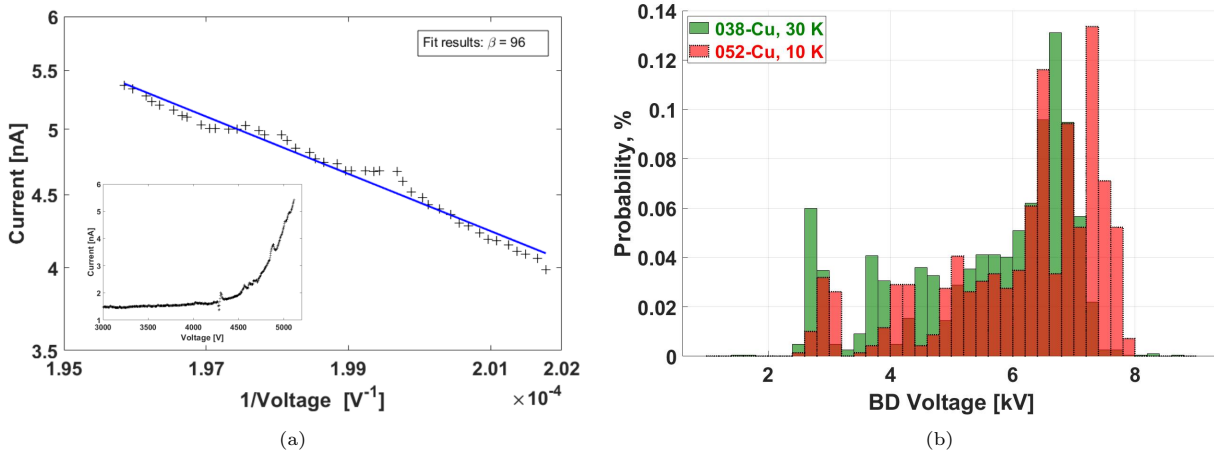


Figure 11: (a) Fowler-Nordheim plot after field emission from 038-Cu fitted to extract the local field enhancement factor. The inset shows the original I-V plot. (b) Histogram of BD voltages for the samples 038-Cu and 052-Cu tested at 30 and 10 K showing a very similar range of BD voltages. It seems that the BD voltages histograms on Fig.11b do not fully overlap. At the highest BD voltages, 052-Cu surpasses 038-Cu exhibiting quite a large number of BDs happening above 7.5 kV. The difference could originate from a lower test temperature (10 vs 30K).

on each electrode agree between the sets, with the slightly larger values for the cryogenically cooled sets. The deviation between the size can be attributed to different conditioning voltages sustained at cold and warm and with this the energy available for the BD to feed the plasma.

Some of the breakdown events were accompanied by the creation of atypical BD spot. The number of such spots increased with reduction of the conditioning temperature, from 25% at 30 K to 53% at 10 K. The parameters of the conditioning process used for both sets were kept the same and both reached similar saturated voltages, illustrated in figure 11b, giving confidence that the temperature difference is strongly related to the twofold increase in the number of atypical spots. Similarly, the morphological data in the table 2 for both sets match very closely, giving large confidence in comparison of the atypical features between the two sets.

These spots are very characteristic, with a very shallow depth and star-like shape instead of circular ones. The size of the star-like feature is harder to measure, but fitting a circle to the largest dark part of the feature give somewhat smaller values than the regular one, but not significantly. The corresponding anode sites are also more shallow than the regular ones, but similar in morphology.

H. Padamsee and J. Knobloch observed the starbursts on BD sites formed in superconducting RF cavity made from Nb and Nb electrodes tested under DC [33]. They proved with SEM and Auger spectroscopy that the starbursts were sites in which a very thin film of fluorine con-

tamination was burnt by plasma ignited during the BD event. Thus, the starburst was a fingerprint left by a plasma cloud in a thin contamination layer. The star-like BDs observed in the present work could also be the fingerprints of a plasma cloud. But they are deeper, i.e. they were left in the metal itself. Cu has much lower melting temperature than Nb: 1085 vs 2477°C and this could be the reason for deeper fingerprint. In the current study, the shallow plasma fingerprint left in the thin surface layer of contamination/oxidation was found beyond the rough circumference of the star-like BD.

We believe therefore that the star burst is the consequence of an unstable emitting tip that ejects molten material in random directions, that lands on the cold surface and freezes rapidly creating such shapes. If melting continues, the regular circle around the crater will form and expand, covering in turn the features created by plasma instabilities initially. In the room temperature experiments, we did not find any traces of the instabilities, however in cryogenic temperatures, the heat is dissipated much more efficiently due to much higher thermal diffusivity, $10^{-4} \frac{m^2}{s}$ at 300 K and $0.2 \frac{m^2}{s}$ at 10 K [34], allowing cryogenically cooled copper to rapidly crystallize on the surface, leaving clear traces that can provide a glimpse to the first stages of the thermal runaway of the tip.

The very distinct morphology of the anode spots from the cathodes is quite baffling, taking into account the standard models for plasma formation and expansion in vacuum [35]. We note that the BD spot diameter for a typical

BD event (e.g. main dark, rough part of the cathode spot) is 4 times larger than the gap size, suggesting that the plasma fills quite a substantial part of the gap between the BD spot. And indeed the cathode spots show clear melting and reshaping of the surface. But looking at the anodes' spots, we find more complicated morphology. The traces from the machining are visible over anode's spot most inner, lighter, disk, indicating no significant melting. Around the disk, we find a dark, rough part that covers or removes the grooves. Radial jets around the anode BD feature, so frequent on the cathode, are missing, which supports the no-melting hypothesis. Lastly, we find no significant differences between room temperature and cryogenically conditioned anode spots. In search for possible explanation for this unusual morphology, we looked at the theories for the trigger mechanism of vacuum breakdown. There are two main proposition for the mechanism related to the source of the gas for ionization. The first one assumes that a cathode related processes are dominant, and the other one hints that the anode is initiating the process [36, 37]. There are experimental and theoretical evidence supporting both hypothesis, but the former is more accepted and experimentally verified in wider range of experimental parameters (e.g. [38]). Adopting this hypothesis and assuming that the plasma originated at a single spot at the cathode and went through a rapid expansion into vacuum, we would expect it to have a spherically symmetric distribution that follows a cosine distribution with respect to the angle to the surface normal, ν [39]. One would thus presume to find the maximum of the plasma density, n , at the center of the anode spot with a quadratic drop with the distance from the center, r [26]:

$$n = C \frac{I_{arc}}{r^2} \cos \nu \quad (2)$$

where C is a constant (for copper $C \approx 10^{13} \frac{1}{Am}$) and I_{arc} is the arc current. This is clearly not the pattern we are observing on the anode surface.

In the majority of studies that measured the angular distributions of plasma plume following vacuum breakdown, large gap systems were used to take better advantage of the granularity of the detectors, assuming that the gap distance has no effect on the results (see for example [39] and references therein). Similarly, in the research investigations into the cathode vs anode-dominated mechanism, the plasma has been analyzed spectroscopically, looking at the evolution of plasma glow, which also required larger gaps (> 1 mm) [38, 40]. These groups observed inter-electrode glow starting from the cathode and thus excluded the anode-dominated BDs hypothesis in their experiments, suggesting that in such configuration, the beam of field emitted electrons is not narrow enough to heat and start evaporation from the anode and that these electrons arriving at the anode have such high energy (> 50 keV) that their probability of gas ionization is negligible.

In our case, the gap is shorter, resulting in smaller

electron energies and more focused beam hitting the anode. Assuming that the emitted current originates from a localized emission site on the cathode that is characterized by the radius of the emission area, r_e , and a region where field is locally enhanced, r_p , it can be shown that the beam radius a distance d from the emitter will be [35]:

$$r_a = 2r_e \left(\beta \frac{d}{r_p} \right)^{1/2} \quad (3)$$

for simplicity we assume that $r_p = r_e = 10$ nm and take the $\beta = 96$, as measured before, this leads to a high space charge region with a radius of $15.3 \mu m$ on the anode surface. It is then reasonable to assume that interaction between expanding plasma and this high space charge region may lead to the formation of local shielded region that can form a small reflective surface, as observed (see r_a at figure 4a and table 2).

While we do not disagree with the importance of the cathode in the initialization of the vacuum breakdowns, we find that a more complicated mechanism is needed to explain the situation in the short gap system. We can speculate that the initial field emission current forms an electron beam that interacts with the emerging and expanding plasma and shields the central region from the melting and perhaps contributes to voluminous distribution of the plasma away from the emission point.

Our study put to the test the hypothesis that the conditioning of copper in high field systems is dominated by material hardening [9]. Firstly, we investigated surface modification with the hardness test, which showed that the hardness is not directly correlated with the conditioning or the surface's ability to retain field. In addition, the sub-surface study of the samples found evidence of noticeable structural differences in the high-field regions. Conditioning, regardless of temperature, resulted in a visible decrease and not increase in the number of dislocation walls. Notably, this effect was stronger in the cold-conditioned sample. We speculate that the ultimate breakdown strength of copper is achieved after a period of surface conditioning to allow for rearrangement of the near-surface crystallographic defects, regardless of the initial state of the surface. This period is longer when one starts with heat-treated, 'soft', copper, and shorter for 'hard', 'as-machined' copper (see [9]). The final hardness and density of dislocations for the optimal surface state are in between the two initial states and the conditioning period, and with it, the number of pulses required for the sub-surface to gradually reorder itself under the stress, is directly related to the distinctiveness between them. This shows again that a more intricate mechanism is behind, and only further study can help validate our results and provide additional information about the high-field conditioning process [41].

References

- [1] D. M. S. Raymond L. Boxman, P. J. M. (Eds.), Handbook of Vacuum Arc Science and Technology. Fundamentals and Applications, Materials science and process technology series, Noyes Publications, 1995.
- [2] CERN, The Compact Linear Collider CLIC - 2018 Summary Report, edited by P.N.Burrows, N.Catalan Lasheras, L.Linssen, M.Petric, A.Robson, D.Shulte, E.Sicking, S.Stapnes (2018). doi:10.23731/CYRM-2018-002. URL <https://e-publishing.cern.ch/index.php/CYRM/issue/view/66>
- [3] A. Descoedres, T. Ramsvik, S. Calatroni, M. Taborelli, W. Wuensch, dc breakdown conditioning and breakdown rate of metals and metallic alloys under ultrahigh vacuum, Physical Review Special Topics - Accelerators and Beams 12 (3) (2009) 032001, publisher: American Physical Society. doi:10.1103/PhysRevSTAB.12.032001. URL <https://link.aps.org/doi/10.1103/PhysRevSTAB.12.032001>
- [4] A. Degiovanni, W. Wuensch, J. Giner Navarro, Comparison of the conditioning of high gradient accelerating structures, Phys. Rev. Accel. Beams 19 (2016) 032001. doi:10.1103/PhysRevAccelBeams.19.032001. URL <https://link.aps.org/doi/10.1103/PhysRevAccelBeams.19.032001>
- [5] A. Descoedres, F. Djurabekova, K. Nordlund, DC breakdown experiments with cobalt electrodes, Tech. rep., CERN, Geneva (2009). doi:10.17181/CLIC-Note-875. URL <http://cds.cern.ch/record/1355401>
- [6] A. Saressalo, Experimental study of the role of extrinsic and intrinsic vacuum arc breakdown mechanisms, Ph.D. thesis, Helsinki U. (2021). URL <http://hdl.handle.net/10138/336482>
- [7] S. Bagchi, D. Perez, Atomistic modeling of the coupling between electric field and bulk plastic deformation in fcc metals, Phys. Rev. Accel. Beams 25 (2022) 033101. doi:10.1103/PhysRevAccelBeams.25.033101. URL <https://link.aps.org/doi/10.1103/PhysRevAccelBeams.25.033101>
- [8] G. Wang, E. I. Simakov, D. Perez, Ab initio investigation of elastic properties of dilute Cu alloys for high-gradient accelerating structures, Journal of Applied Physics 132 (17) (2022) 175112. doi:10.1063/5.0106880. URL <https://doi.org/10.1063/5.0106880>
- [9] A. Korsbäck, F. Djurabekova, L. M. Morales, I. Profatilo, E. Rodriguez Castro, W. Wuensch, S. Calatroni, T. Ahlgren, Vacuum electrical breakdown conditioning study in a parallel plate electrode pulsed dc system, Physical Review Accelerators and Beams 23 (3) (2020) 033102. doi:10.1103/PhysRevAccelBeams.23.033102.
- [10] A. S. Pohjonen, F. Djurabekova, K. Nordlund, A. Kuronen, S. P. Fitzgerald, Dislocation nucleation from near surface void under static tensile stress in Cu, Journal of Applied Physics 110 (2) (2011) 023509. doi:10.1063/1.3606582. URL <https://doi.org/10.1063/1.3606582>
- [11] W.-W. Pang, P. Zhang, G.-C. Zhang, A.-G. Xu, X.-G. Zhao, Dislocation creation and void nucleation in FCC ductile metals under tensile loading: A general microscopic picture, Scientific Reports 4 (1) (2014) 6981, number: 1 Publisher: Nature Publishing Group. doi:10.1038/srep06981. URL <https://www.nature.com/articles/srep06981>
- [12] K. Nordlund, F. Djurabekova, Defect model for the dependence of breakdown rate on external electric fields, Phys. Rev. ST Accel. Beams 15 (2012) 071002. doi:10.1103/PhysRevSTAB.15.071002.
- [13] V. Zadin, M. Veske, S. Vigonski, V. Jansson, J. Muszinsky, S. Parviainen, A. Aabloo, F. Djurabekova, Simulations of surface stress effects in nanoscale single crystals, Modelling and Simulation in Materials Science and Engineering 26 (3) (2018) 035006. doi:10.1088/1361-651X/aaa928. URL <https://dx.doi.org/10.1088/1361-651X/aaa928>
- [14] E. Z. Engelberg, Y. Ashkenazy, M. Assaf, Stochastic model of breakdown nucleation under intense electric fields, Phys. Rev. Lett. 120 (Mar 2018). doi:10.1103/PhysRevLett.120.124801. URL <https://link.aps.org/doi/10.1103/PhysRevLett.120.124801>
- [15] E. Z. Engelberg, J. Paszkiewicz, R. Peacock, S. Lachmann, Y. Ashkenazy, W. Wuensch, Dark current spikes as an indicator of mobile dislocation dynamics under intense dc electric fields, Phys. Rev. Accel. Beams 23 (12) (2020) 123501. doi:10.1103/PhysRevAccelBeams.23.123501.
- [16] J. Paszkiewicz, Studies of breakdown and pre-breakdown phenomena in high-gradient accelerating structures, Ph.D. thesis, Oxford U. (2020). URL <https://ora.ox.ac.uk/objects/uuid:2845c530-573f-4616-942d-f510781ad4cf/files/djs956f882>
- [17] Y. Ashkenazy, A. Yasha, O. Cohen, I. Popov, Observations of dislocations in soft cu samples exposed to high fields, in: 10th International Workshop on the Mechanisms of Vacuum Arcs (MeVArc2023), Chania, Crete, 2022. URL <https://indico.cern.ch/event/1099613/contributions/4969676/>
- [18] M. Nasr, E. Nanni, M. Breidenbach, S. Weathersby, M. Orinno, S. Tantawi, Experimental demonstration of particle acceleration with normal conducting accelerating structure at cryogenic temperature, Physical Review Accelerators and Beams 24 (9) (2021) 093201, publisher: American Physical Society. doi:10.1103/PhysRevAccelBeams.24.093201. URL <https://link.aps.org/doi/10.1103/PhysRevAccelBeams.24.093201>
- [19] M. Jacewicz, J. Eriksson, R. Ruber, S. Calatroni, I. Profatilo, W. Wuensch, Temperature-Dependent Field Emission and Breakdown Measurements Using a Pulsed High-Voltage Cryosystem, Physical Review Applied 14 (6) (12 2020). doi:10.1103/PhysRevApplied.14.061002.
- [20] M. Aicheler, P. Burrows, M. Draper, T. Garvey, P. Lebrun, K. Peach, N. Phinney, H. Schmickler, D. Schulte, N. Toge, A Multi TeV Linear Collider based on CLIC technology: CLIC Conceptual Design Report, Tech. rep., CERN (2012). doi:10.5170/CERN-2012-007. URL <https://cds.cern.ch/record/1500095/files/CERN-2012-007.pdf?version=1>
- [21] M. Malabaila, Operating procedure for the MEG solvent degreasing machine, Tech. rep. (2014).
- [22] I. Profatilo, X. Stragier, S. Calatroni, A. Kandratsyev, E. Rodriguez Castro, W. Wuensch, Breakdown localisation in a pulsed DC electrode system, Nuclear Inst. and Methods in Physics Research, A 953 (August) (2020) 163079. doi:10.1016/j.nima.2019.163079. URL <https://doi.org/10.1016/j.nima.2019.163079>
- [23] I. Profatilo, W. Wuensch, S. Calatroni, Behaviour of copper during initial conditioning in the pulsed DC system, CLIC Note (2019). URL <https://cds.cern.ch/record/2703709?ln=en>
- [24] A. Saressalo, A. Kyrtsakis, I. Profatilo, J. Paszkiewicz, S. Calatroni, W. Wuensch, F. Djurabekova, Classification of vacuum arc breakdowns in a pulsed dc system, Physical Review Accelerators and Beams 23 (2) (2020) 023101. doi:10.1103/PhysRevAccelBeams.23.023101.
- [25] A. Saressalo, I. Profatilo, W. L. Millar, A. Kyrtsakis, S. Calatroni, W. Wuensch, F. Djurabekova, Effect of dc voltage pulsing on high-vacuum electrical breakdowns near Cu surfaces, Physical Review Accelerators and Beams 23 (11) (2020) 113101. doi:10.1103/PhysRevAccelBeams.23.113101.
- [26] A. Anders, Cathodic arcs : from fractal spots to energetic condensation, Springer series on atomic, optical, and plasma physics ; 50, Springer, New York ;, 2008.
- [27] A. Saressalo, Experimental study of the role of extrinsic and intrinsic vacuum arc breakdown mechanisms, Ph.D. thesis, University of Helsinki, Helsinki (2021). URL <https://ethesis.helsinki.fi>
- [28] T. Sonar, S. Lomte, C. Gogte, Cryogenic treatment of metal –

- a review, *Materials Today: Proceedings* 5 (11, Part 3) (2018) 25219–25228. doi:<https://doi.org/10.1016/j.matpr.2018.10.324>.
URL <https://www.sciencedirect.com/science/article/pii/S2214785318326282>
- [29] Z. Shengquan, W. Bing, W. Shizhuo, Z. Changzhong, W. Xijing, Z. Zhongke, Effect of cryogenic treatment on extruded copper structures, *IOP Conference Series: Materials Science and Engineering* 688 (3) (2019) 033087. doi:10.1088/1757-899X/688/3/033087.
URL <https://dx.doi.org/10.1088/1757-899X/688/3/033087>
- [30] I. Popov, Y. Ashkenazy, A. Yashar, I. Profatilova, E. Rodriguez Castro, W. Wuensch, Identification of dislocation structure in cu electrodes, in: *9th International Workshop on the Mechanisms of Vacuum Arcs (MeVArc 2021)*, Online, 2021.
URL <https://indico.cern.ch/event/966437/contributions/4245452/>
- [31] A. D. Cahill, J. B. Rosenzweig, V. A. Dolgashev, S. G. Tantawi, S. Weathersby, High gradient experiments with X-band cryogenic copper accelerating cavities, *Phys. Rev. Accel. Beams* 21 (2018) 102002. doi:10.1103/PhysRevAccelBeams.21.102002.
URL <https://link.aps.org/doi/10.1103/PhysRevAccelBeams.21.102002>
- [32] T. E. Stern, B. S. Gossling, R. H. Fowler, Further studies in the emission of electrons from cold metals, *Proceedings of the Royal Society of London. Series A, Containing Papers of a Mathematical and Physical Character* 124 (795) (1997) 699–723, publisher: Royal Society. doi:10.1098/rspa.1929.0147.
URL <https://royalsocietypublishing.org/doi/10.1098/rspa.1929.0147>
- [33] H. Padamsee, J. Knobloch, The nature of field emission from microparticles and the ensuing voltage breakdown, *AIP Conf. Proc.* 474 (1) (1999) 212–248. doi:10.1063/1.59014.
- [34] J. Ekin, *Experimental Techniques for Low-Temperature Measurements: Cryostat Design, Material Properties and Superconductor Critical-Current Testing*, Oxford University Press, 2006. doi:10.1093/acprof:oso/9780198570547.001.0001.
URL <https://doi.org/10.1093/acprof:oso/9780198570547.001.0001>
- [35] P. G. Slade, *The Vacuum Interrupter: Theory, Design, and Application*, 2nd Edition, CRC Press, Boca Raton, 2020. doi:10.1201/9780429298912.
- [36] T. Utsumi, Cathode- and Anode-Induced Electrical Breakdown in Vacuum, *Journal of Applied Physics* 38 (7) (2004) 2989–2997. doi:10.1063/1.1710038.
URL <https://doi.org/10.1063/1.1710038>
- [37] D. K. Davies, M. A. Biondi, The Effect of Electrode Temperature on Vacuum Electrical Breakdown between Plane-Parallel Copper Electrodes, *Journal of Applied Physics* 39 (7) (2003) 2979–2990. doi:10.1063/1.1656718.
URL <https://doi.org/10.1063/1.1656718>
- [38] Z. Zhou, A. Kyrtsakis, Z. Wang, Y. Li, Y. Geng, F. Djurabekova, Effect of the anode material on the evolution of the vacuum breakdown process, *Journal of Physics D: Applied Physics* 54 (1 2021). doi:10.1088/1361-6463/abbbb7.
- [39] A. Anders, G. Y. Yushkov, Angularly resolved measurements of ion energy of vacuum arc plasmas, *Applied Physics Letters* 80 (14) (2002) 2457–2459. doi:10.1063/1.1468271.
URL <https://doi.org/10.1063/1.1468271>
- [40] D. K. Davies, M. A. Biondi, Emission of electrode vapor resonance radiation at the onset of dc breakdown in vacuum, *Journal of Applied Physics* 48 (10) (2008) 4229–4233. doi:10.1063/1.323407.
URL <https://doi.org/10.1063/1.323407>
- [41] M. Coman, M. Jacewicz, D. Dancila, In situ resistivity measurement of metal surfaces to track down dislocations caused by high field conditioning, *International Journal of Microwave and Wireless Technologies* (2023) 1–9doi:10.1017/S1759078723001411.